MASSES, LUMINOSITIES, AND DYNAMICS OF GALACTIC MOLECULAR CLOUDS

P. M. Solomon
A. R. Rivolo
T. J. Mooney
J. W. Barrett
L. J. Sage

Astronomy Program, State University of New York—Stony Brook

Star formation in galaxies takes place in molecular clouds and the Milky Way is the only galaxy in which it is possible to resolve and study the physical properties and star formation activity of individual clouds. In this paper we describe and analyze the masses, luminosities, dynamics and distribution of molecular clouds, primarily giant molecular clouds in the Milky Way. The observational data sets are the Massachusetts–Stony Brook CO Galactic Plane Survey and the *IRAS* far IR images. The molecular mass and infrared luminosities of galactic clouds are then compared with the molecular mass and infrared luminosities of external galaxies.

Section 1 describes how molecular clouds are observationally defined from the CO survey. We then show in section 2 that molecular clouds have well defined empirical laws governing their size–linewidth and virial mass–CO luminosity relationships (Solomon *et al.* 1986a). The virial mass–CO luminosity law establishes a physical basis for the use of CO as a tracer of molecular cloud mass, primarily H_2. The size–linewidth law combined with the dynamical mass from the virial theorem leads to mass–linewidth and CO luminosity–linewidth laws. Section 3 presents the molecular cloud mass spectrum.

In order to determine the current star formation activity in GMC's we have measured their far IR luminosity from a comparison of the *IRAS* and CO data. Section 4 shows that the IR luminosity is proportional to the CO luminosity and that the (IR luminosity / cloud mass) is independent of mass. There is a maximum to the $L_{IR}/M(H_2)$ ratio in galactic molecular clouds indicating that star formation activity is well regulated within the clouds. Section 5 briefly discusses the comparison between far IR and CO emission on a galactic scale and section 6 shows a face on picture of molecular clouds in the galaxy. In section 7 we briefly summarize our results on far IR and CO luminosities in external galaxies. We compare the star formation activity in isolated and interacting galaxies with that of galactic molecular clouds. The interacting galaxies have (IR luminosity / molecular mass) ratios substantially higher than any galactic molecular cloud.

1. CO Observations and Cloud Definition

The CO survey observations were carried out during 1981 and 1982 on the FCRAO

Carol J. Lonsdale Persson (Editor)
Star Formation in Galaxies

14 meter antenna operating at a frequency of 115.271 GHz (HPBW = 47 arc seconds). Approximately 40,000 CO spectra were obtained between the limits of 8° to 90° in longitude, −1° to +1° in latitude and −100 to +200 km·s^{-1} in velocity with a typical rms noise level of 0.35 K. The survey spacing of 3 arc minutes (over the range ℓ = 18° to 54°) was chosen to enable measurement of essentially all molecular clouds inside the solar circle with size greater than 20 pc. For example on the far side of the galaxy at distances of 14 kpc the spacing is 13 pc; on the near (wrt the tangent point) side in the molecular ring at a distance of 4 kpc the spacing is 3.5 pc. A more complete discussion of the observations and calibration procedures along with maps of the complete data in latitude-velocity space is in Sanders *et al.* (1986); longitude-velocity maps and spatial (longitude-latitude) maps at fixed velocities are given in Clemens *et al.* (1986) and Solomon *et al.* (1986b). Inspection of the actual survey contours in the above references shows that many clouds easily stand out from the background and can be defined with little difficulty. However there are also regions of strong emission with blending of features in which the definition of cloud boundaries in the three dimensional (ℓ, b, v) space is complicated and may be subject to different interpretations by different observers. In our first analysis of the Massachusetts–Stony Brook CO Galactic Plane Survey (Solomon, Sanders and Rivolo 1985) we overcame the boundary problem by defining CO sources, representing the cores of molecular clouds, as local maxima in ℓ, b, v space. We showed that the galaxy had two populations characterized by (1) warm molecular cloud cores with one-quarter of the population and about one-half of thte emission; they exhibit nonaxisymmetric galactic distribution, are clearly associated with H II regions, appear to be clustered, and are a spiral arm population; and (2) cold molecular cloud cores containing three-quarters of the total number; they are a widespread disk population located both in and out of spiral arms.

In this work we adopt a procedure which unambiguously defines cloud boundaries in three dimensions in order to obtain an objective cloud data set and to study cloud structure and dynamics. Clouds are defined as closed surfaces in the three dimensional space at fixed intensity levels T_R^* = 3, 4, 5, 6, 7 K. The galactic plane emission is thus broken up into a set of discrete clouds for each intensity. For the purpose of this analysis a cloud was required to have a minimum total integrated intensity summed over all locations inside the surface of 40 K·km·s^{-1} for T_R^* = 6 and 7 K and 60 K·km·s^{-1} for T_R^* = 4 and 5 K. Each set corresponds to a cloud catalog containing about 400 clouds. There are about 1,000 clouds smaller than the minimum. Large sections of the galactic plane are blended at the 3 K level with features extending over as much as 5° and 60 K·km·s^{-1}. By contrast there is very little blending of the surfaces at the 6 K level. The 4 K catalog was adopted except for the most confused regions between longitudes of 8° and 32° and velocities $v > 60$ km·s^{-1}. Here a selection was made of the lowest intensity surface cloud which was not severely blended. A quantitative measure of the cloud asymmetry was utilized to eliminate spatially blended clouds. The final catalog is thus composed of a mixture of clouds defined at the 4, 5 and 6 K levels. Above longitudes of 54°, where the emission is weaker, the 3 K

clouds were substituted for the 4 K clouds.

Each cloud in the final catalog is described by a set of parameters including the location of the emission peak in ℓ, b, v space, the minimum and maximum extent (in ℓ, b, v) of the emission surface, a total CO flux inside the surface, a galactocentric radius R determined from circular rotation, and the rms dispersions from the means in all three coordinates. There is a two fold (near-far) distance ambiguity for all kinematic distances in the inner galaxy. We have resolved the ambiguity by utilizing a boot strap process based on the cloud physical properties measured for a subset of clouds with known distances which serve as calibrators. The calibrator clouds include those with small near-far distance ratios (tangent point clouds), and clouds which can be assigned either near or far on the basis of an association with an H II region (Downes 1980) with a radio frequency absorption line for which an assignment has been made.

2. The Size–Linewidth and Virial Mass–CO Luminosity Relations

For the calibrators a direct relationship between cloud size, defined as the geometric mean of the ℓ–b dispersions [$S = D\tan(\sqrt{\sigma_\ell \sigma_b})$] and the velocity linewidth, is established. Although the cloud boundaries have been defined at the particular level ($T_R^* = 3, 4, 5, 6,$ 7 K) we have included all emission down to the 1 K level within a cube circumscribing the cloud boundaries for the purpose of determining the cloud size, linewidth and luminosity. Measuring S in parsecs we find (see Figure 1)

$$\sigma_v = \left(\frac{S}{1.01}\right)^{0.5} \quad (\mathrm{km \cdot s^{-1}}) \tag{1}$$

with a logarithmic dispersion in σ_v of ± 0.13 or 40%.

Near or far distances to all remaining clouds in the final list were assigned using three criteria: 1) choosing the distance with the better fit to the size-linewidth relation, 2) choosing the near side if the far distance places the cloud more than 150 pc out of the plane, and 3) choosing near or far based on the best fit for the scale height of the emission in the longitude and velocity range of the cloud. The third method utilizes the well determined value for the half width at half maximum of the molecular layer of 60 parsecs (see *e.g.* Sanders, Solomon and Scoville, 1984). The details of these methods are explained elsewhere (Solomon *et al.* 1986a). For the purposes of this paper the accuracy of distance assignments is not critical since the result using only calibrator clouds is virtually identical to that using all clouds.

For each of the clouds a virial theorem mass can now be determined from the measured velocity and size dispersion

$$M_{VT} = \frac{3\, f_p\, S\, {\sigma_v}^2}{G} \quad (\mathrm{M_\odot})$$

where f_p is a projection factor (taken herein as π, this being consistent with a cylindrical truncation of spherically symmetric clouds), and $G = 1/232$ in units of $\mathrm{km \cdot s^{-1}}$ and

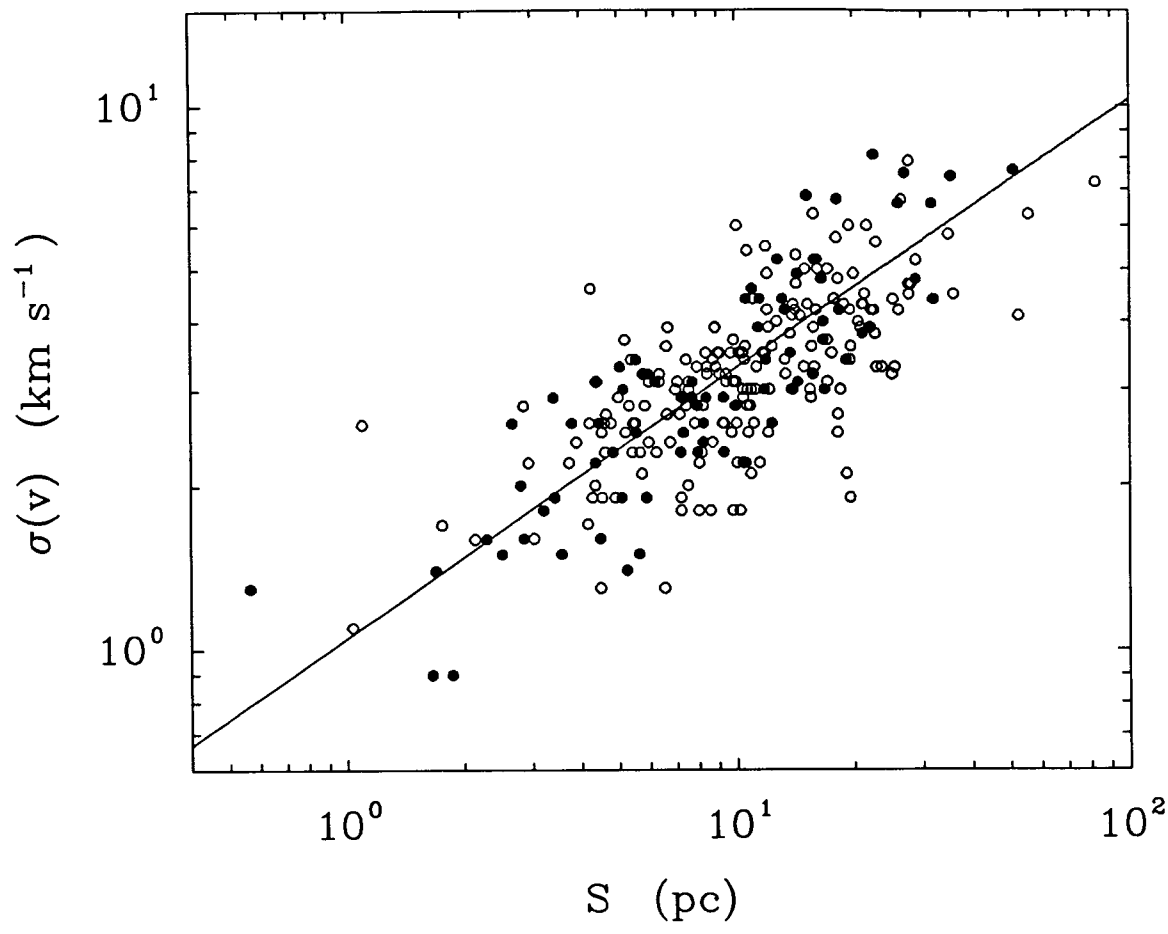

Figure 1. Molecular cloud velocity dispersion $\sigma(v)$ as a function of size dispersion S for 250 clouds in the inner galaxy. The solid circles are calibrator clouds with known distances and the open circles are for clouds with the near-far distance ambiguity resolved by the three techniques discussed in the text. The fit line is $\sigma_v = (S/1.0)^{0.5}$ km $\cdot$ s^{-1}. For virial equilibrium the 0.5 power law requires clouds of constant surface density.

parsecs. In addition, a cloud's CO luminosity is obtained directly from the survey data within the cloud boundaries as

$$L_{CO} = D^2 \int\int\int T_R^*(\ell, b, v)\, d\ell\, db\, dv \quad (\mathrm{K \cdot km \cdot s^{-1} \cdot pc^2}) \tag{2}$$

where $T_R^*(\ell, b, v)$ is the antenna temperature at location (ℓ, b, v). Figure 2 shows the virial mass as a function of CO luminosity for all clouds with calibrators shown as filled symbols. A least squares fit to all of the data shows an extremely tight power-law fit over a range of four decades given by

$$M_{VT} = 42\ (L_{CO})^{0.81} \quad (\mathrm{M_\odot}) \tag{3}$$

with a dispersion of 0.14 in $\log(M_{VT})$ or 38% in M_{VT}.

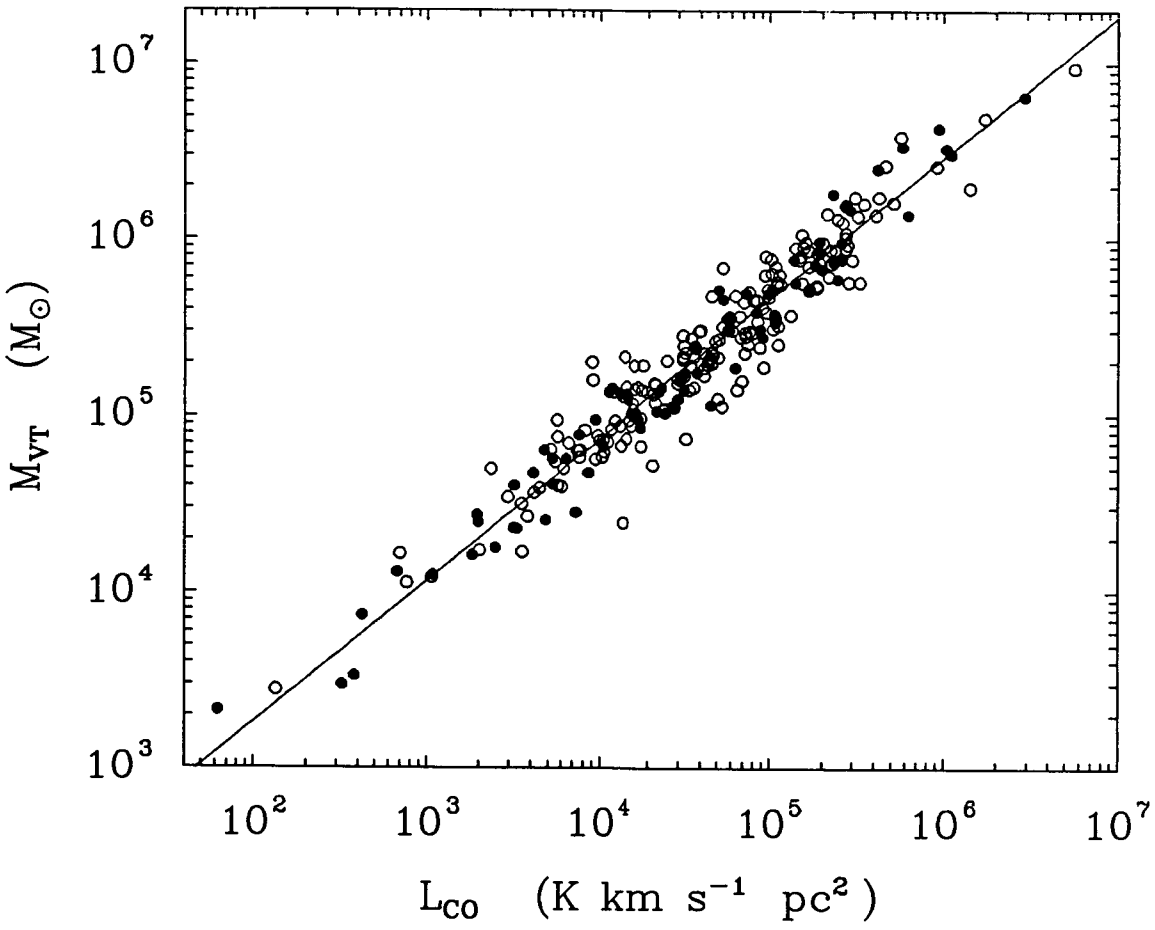

Figure 2. The Virial Mass–CO Luminosity relation for molecular clouds. The clouds range in distance from 1 to 15 kpc and in flux over more than two orders of magnitude. The solid circles and open circles are the same as in Figure 1. The fit is $M_{VT} = 42\,(L_{CO})^{0.81}$ $M_\odot$. For a given L_{CO} the dispersion in M_{VT} is 0.13 in the log.

The observed cloud mass–CO luminosity relation can be translated into a molecular hydrogen column density $N(H_2)$ as a function of the average CO integrated intensity over the cloud velocity range Δv, $\bar{I} = \int_{\Delta v} T\, dv$. The mass is the product of the mean column density and the surface area; the luminosity is the product of $\bar{I}$ and the surface area. Letting $N(H_2) = a\,\bar{I}$, we find $a = 4.7$, 3.1 and $2.0(10)^{20}$ for CO luminosities of 10^4, 10^5 and 10^6 K·km·s^{-1}·pc^2. Thus, although the mass is not strictly a linear function of CO luminosity, the conversion factor varies by only a factor of two between clouds of mass 5×10^4 and 2×10^6 $M_\odot$. We adopt $a = 3.1$ as the effective conversion factor for clouds of mass 3×10^5 $M_\odot$ which are close to the median of the mass distribution.

The only other technique which has determined the CO luminosity to mass conversion factor for giant molecular clouds with $m > 10^5$ $M_\odot$ uses the observed γ-ray flux resulting

from cosmic ray interactions with hydrogen molecules. As summarized in Table 1 for the Orion Molecular Cloud $a = 2.6 \pm 0.8$ and for the galactic plane emission between $R = 5$ kpc and $R = 10$ kpc, $a = 2.8 \pm 1$ (Bloemen *et al.* 1984, 1986). The conversion factor based on the variation of optical extinction measured along the lines of sight with measured CO or ^{13}CO integrated intensity also gives good agreement although the clouds are typically of lower mass.

The close agreement of these conversion factors with our dynamical measurement demonstrates that the assumption of virial equilibrium in the clouds is correct. Molecular clouds are therefore bound by self gravity and not by pressure equilibrium with a hot phase of the ISM.

The agreement between these techniques and between the local and molecular ring calibrations provides an empirical basis for the measurement of the total mass of molecular hydrogen in the galactic disk (see *e.g.* Sanders, Solomon and Scoville, 1984 and Table 2). The agreement between the dynamical conversion factor which is heavily weighted to clouds in the molecular ring at $R = 5$ kpc, the γ-ray conversion factor determined for a mixture of the molecular ring and relatively local clouds and the γ-ray conversion factor determined for the nearby Orion molecular clouds shows that a constant conversion factor for the galactic disk between $R = 4$ kpc and $R = 10$ kpc may be used to determine the total H_2 mass. There is no evidence of a radial gradient in the conversion factor between $R = 5$ and 10 kpc as suggested by Bhat *et al.* (1985) and Blitz and Shu (1980).

One of the more interesting empirical results which follows directly from the size-linewidth relation (equation 1) and the assumption of virial equilibrium, is the constant surface density of the clouds $\Sigma = 230 \ M_\odot/pc^2$. Equivalently the mass-velocity law is

$$M = 2230 \ \sigma_v{}^4 \quad (M_\odot) \tag{4}$$

Expressed in terms of CO luminosity using equation 3 (Figure 2) yields a relation between velocity-width and size analogous to the Fisher-Tully or Faber-Jackson relation for galaxies

$$L_{CO} = 143 \ \sigma_v{}^5 \quad (K \cdot km \cdot s^{-1} \cdot pc^2) \tag{5}$$

The empirical mass-luminosity law (equation 3 and Figure 2) provides a basis for understanding the use of optically thick CO emission as a tracer of mass, primarily molecular hydrogen, in interstellar clouds. Both the existence and the form of the mass-luminosity law are a consequence of the structure and gravitational equilibrium of giant molecular clouds. If we assume that a cloud consists of a large number of small, optically thick regions (clumps), then emission intensity, T_R^*, along a line of sight at a velocity v will be proportional to the filling factor of the clumps at v and the temperature of the clumps T. For a Gaussian line profile the average surface brightness of the cloud is $\bar{I} = (2\pi)^{1/2} T_0 \sigma_v$ where σ_v is the velocity dispersion and T_0 is the peak intensity at the line center averaged over the cloud. The average filling factor of the cloud at line center is T_0/T. The CO luminosity is then the product of the surface area $3\pi S^2$ and the surface brightness

$$L_{CO} = 3\sqrt{2} \ \pi^{3/2} \ T_0 \ \sigma_v \ S^2 \tag{6}$$

TABLE 1

CALIBRATION OF CO INTEGRATED INTENSITY WITH H_2 COLUMN DENSITY

Method	Location	$a = \overline{N}(H_2)/\overline{I}_{CO}$ $(cm^{-2}/K \cdot km \cdot s^{-1})$	References
$A_V \leq 4$ (in dark clouds)	Local	$2.2(10)^{20}$	Dickman 1975
$A_V \geq 5$	Local	$5.0(10)^{20}$	Liszt 1982
$A_V > 5$	Local	$3.6(10)^{20}$	Sanders, Solomon & Scoville 1984
γ rays	Orion	$2.6(10)^{20}$	Bloemen *et al.* 1984
γ rays	$5 \leq R \leq 10$ kpc	$1.0(10)^{20}$	Bhat *et al.* 1985
γ rays	$5 \leq R \leq 10$ kpc	$2.8(10)^{20}$	Bloemen *et al.* 1986
Virial Theorem	$4 \leq R \leq 8$ kpc	$3.1(10)^{20}$	Solomon *et al.* 1986a

TABLE 2

TOTAL GALACTIC H_2 MASS FOR $2 < R < 10$ kpc

Reference	M $(10^9\ M_\odot)$	a $(cm^{-2}/K \cdot km \cdot s^{-1})$
Scoville & Solomon (1975)	1–3	—
Gordon & Burton (1976)	2.1	—
Solomon, Sanders & Scoville (1979)	3.9	5×10^{20}
Thaddeus & Dame (1984)	0.7	$(1\text{–}2) \times 10^{20}$
Sanders, Solomon & Scoville (1984)	2.6	3.6×10^{20}
Bronfman *et al.* (1986)	1.3†	2.8×10^{20}
This Work	2.0‡	3.0×10^{20}

† The difference between this and 2.0 is primarily due to a different weighting used to obtain the radial emissivity and to a 20% lower CO intensi ty calibration.

‡ The emissivity has been calculated using equal weight p er unit of projected face on area for each radial bin.

Combining equation (6) with the virial theorem, and utilizing the empirical size-linewidth relation (equation 1) yields a mass-luminosity relation

$$M_{VT} = 174 \left(\frac{L_{CO}}{T_0}\right)^{4/5} \quad (7)$$

For the clouds in our catalog T_0 ranges from 5 K to about 15 K with a mean of about 7 K which gives $M_{VT} = 37 \left(L_{CO}\right)^{4/5}$ in close agreement with the empirical results in equation 3. Thus the effective conversion factor from luminosity to mass is lower for hotter clouds than for cooler ones, and is lower for more luminous or massive clouds. For a fixed luminosity the mass-to-luminosity ratio can be expressed as a function of the average density $\bar{\rho} = 100/S$ ($M_\odot$ pc^{-3}).

$$\left(\frac{M_{VT}}{L_{CO}}\right) = 12 \frac{(\bar{\rho})^{1/2}}{T_0} \quad (8)$$

Thus the small scatter in Figure 2 is evidence of a fairly small scatter in the mean density of the clouds at a fixed luminosity.

3. The Molecular Cloud Mass Spectrum

Figure 3 shows the mass spectrum of clouds $dN/dm \propto m^{-3/2}$. This is consistent with previous determinations by Solomon and Sanders (1980), Liszt and Burton (1981), and Sanders *et al.* (1985) although it is based on a much larger sample of clouds. The turnover below $m = 5 \times 10^4$ $M_\odot$ is due to the undercounting of clouds, (even warm clouds) on the far side of the galaxy with diameter < 16 pc. The mass fraction of clouds per logarithmic mass interval $m \cdot dN(m)/d\log m \propto m^{1/2}$ demonstrating that most of the mass in molecular clouds is in the high end of the spectrum (Solomon and Sanders, 1980).

As can be seen from Figure 4 the most massive clouds are a few million solar masses and the single most massive object just below 10^7 $M_\odot$.

4. Far Infrared Luminosity of Galactic Molecular Clouds

The *IRAS* survey at 60 μm and 100 μm has an angular resolution similar to that of the Massachusetts–Stony Brook CO Survey of the Galactic Plane. Although the far infrared emission is severely blended it is possible to utilize the velocity information of the CO survey to identify individual molecular cloud/H II region complexes in the far IR. The far IR luminosity originating from newly formed stars in, or associated with, the molecular cloud can then be determined from the *IRAS* maps utilizing the distance to the molecular cloud. The most luminous and hottest molecular clouds (with high peak CO intensity) are readily apparent on the *IRAS* 100 and 60 micron images. Most of the warm molecular clouds have IR counterparts which correspond to H II regions in or on the border of the clouds. An overlay of the locations of the predefined molecular clouds on the

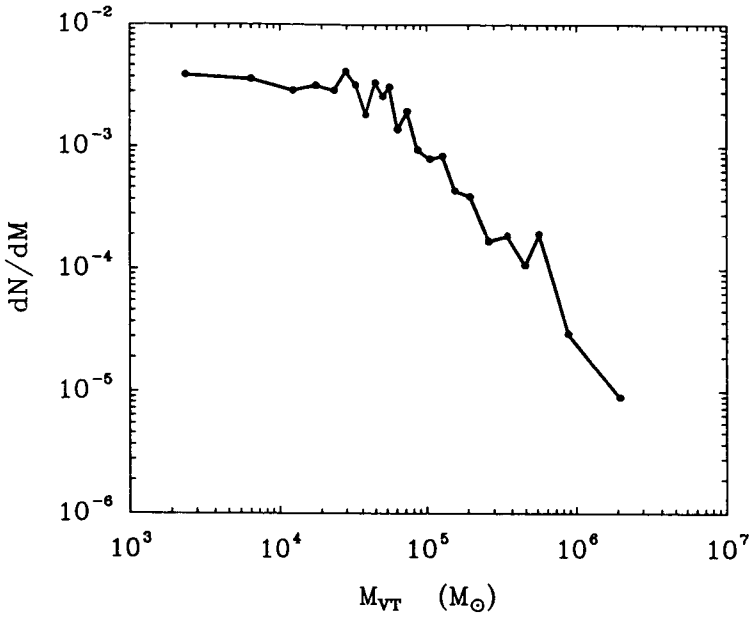

Figure 3. The molecular cloud mass spectrum dN/dm. A fit above 7×10^4 $M_\odot$ gives $dN/dm \propto m^{-3/2}$ (see text). There are 15 clouds in each bin and thus the standard deviation of each point is $\pm 24\%$. The turnover at low mass is due to undercounting of smaller clouds in the more distant parts of the galactic disk.

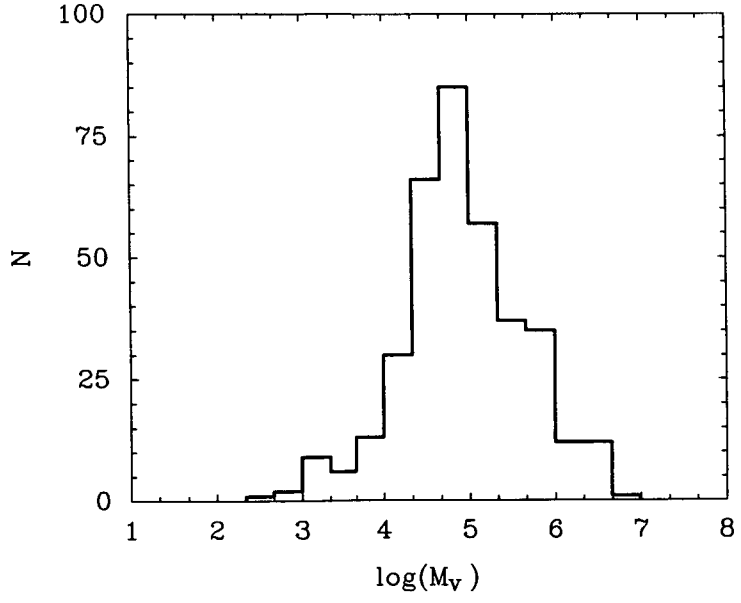

Figure 4. The number of clouds as a function of virial mass in the sample.

IRAS 60 and 100 micron galactic plane images shows a very good, although not complete, correspondence. In particular, almost all of the CO clouds with high CO luminosity and peak intensity above 10 K have obvious IR counterparts. However in regions of the galactic plane where there is a substantial overlap of several strong CO clouds at different velocities,

the infrared emission associated with each cloud may be difficult to separate. We have therefore picked a subset of molecular clouds which are the dominant feature in velocity space over their latitude and longitude extent. For each CO defined cloud a detailed comparison was carried out with the *IRAS* maps smoothed to 3 arc minute resolution. The boundaries of the molecular cloud were slightly adjusted to include *IRAS* sources which were sometimes at the edge of the cloud. In order to be certain that the infrared emission was associated with the velocities of the candidate CO cloud, an interactive program was developed which displayed the average CO spectral line profile over any specified region of (ℓ, b) space. The program would then calculate the total CO flux within the velocity and spatial limits of the cloud and the IR flux above the background but within the cloud boundaries. The IR background which consists principally of galactic background not associated with the candidate cloud and some contribution from the zodical light at 60 microns, was measured by three techniques. The first consists of a point by point comparison of the IR flux as a function of the CO flux.

As can be seen in the example in Figure 5, there is substantial far IR emission uncorrelated with the CO integrated intensity below about 40 $\mathrm{K \cdot km \cdot s^{-1}}$. This uncorrelated emission provides a measure of the background level with respect to the molecular clouds. Similar correlations can be carried out for the restricted velocity range of a single cloud. The second technique finds the background by measuring the radially averaged IR profile around a source associated with a CO cloud. The radially averaged IR flux generally decreases approximately exponentially approaching a background level about two or three scale lengths from the peak. This technique works only for strong or well defined sources. The third method is a standard clipping (κ-σ) technique which iteratively finds the background by eliminating signals more than two standard deviations above the mean.

Figure 6 shows the far infrared luminosity as a function of the CO luminosity for 46 clouds. The clouds range in flux over two orders of magnitude and in luminosity over three orders of magnitude. They include such well known objects as M17, W51, and W43, as well as many previously uncatalogued molecular clouds. A formal fit shows that the infrared luminosity is proportional to the first power of the CO luminosity.

$$L_{IR} = 14\ (L_{CO})^{0.97 \pm 0.08} \quad [L_\odot] \tag{11}$$

The molecular cloud mass M can be obtained from equation 3. Figure 7 shows the ratio of infrared luminosity to cloud mass as a function of the mass. There is a substantial degree of scatter with L_{IR}/M varying from about 1 to 12 with the only significant exception being the M17 cloud with a $L_{IR}/M = 23$. Our cloud defining algorithms have broken the M17 complex into two regions. The well known and strong H II region is associated with a molecular cloud of 2×10^5 $\mathrm{M_\odot}$ and the remainder of the complex is in a cloud which we refer to as M17B with mass of 7×10^5 $\mathrm{M_\odot}$ and a very low luminosity to mass ratio. If we combine these two clouds into one, the ratio becomes 5, near the mean of all other clouds.

The most interesting feature of Figure 7 is the lack of dependence of L_{IR}/M on the cloud mass itself. The star formation rate per unit of available molecular mass is thus

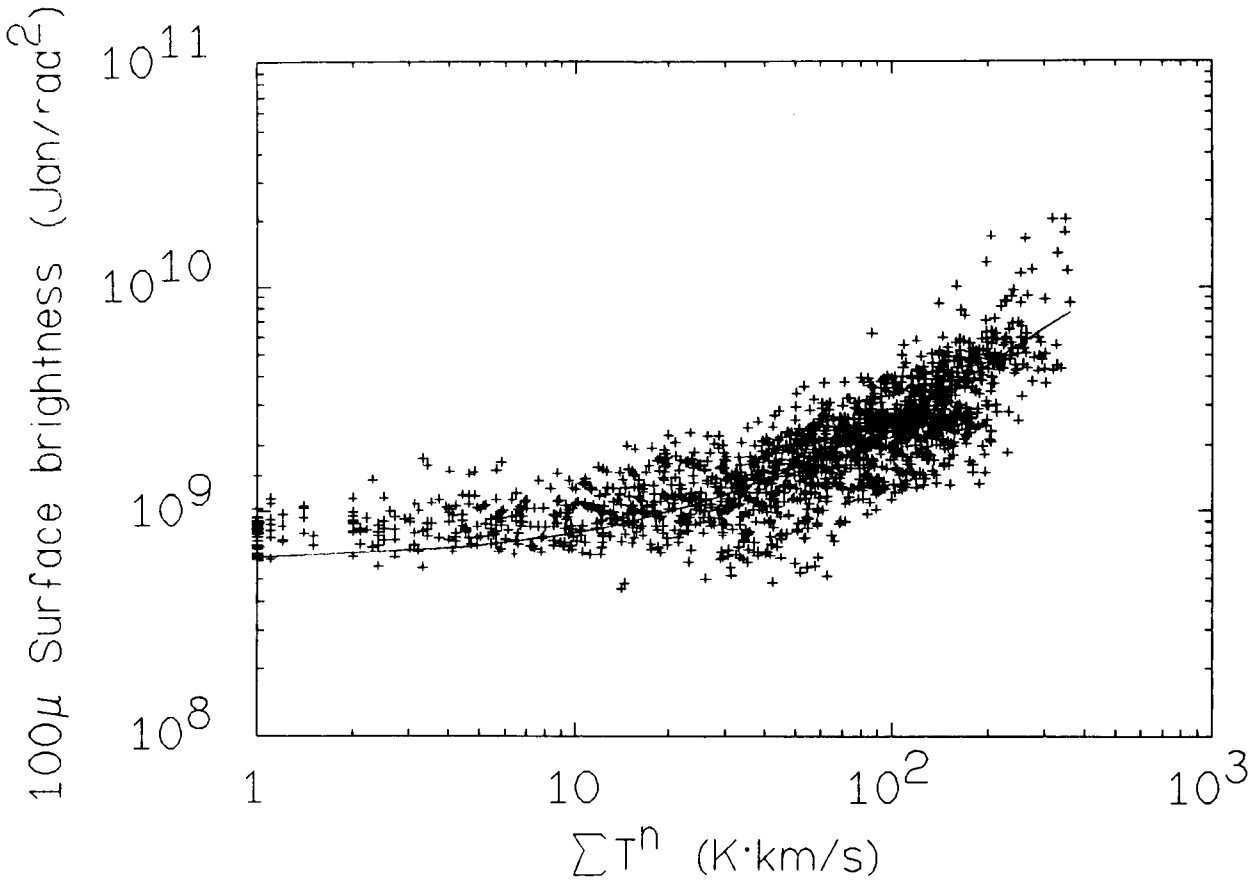

Figure 5. A point by point correlation of IR brightness as a function of CO integrated intensity ($T_R^* > 1$ K; $-40 < v < +140$ km $\cdot$ s^{-1}) for a 2° by 2° region of the galactic plane between $\ell = 29°$ to 31°, $b = -1°$ to $+1°$. There is substantial far IR emission uncorrelated with CO integrated intensity below about 40 K $\cdot$ km $\cdot$ s^{-1}, which provides an estimate of the IR background wrt the molecular clouds. The 100 micron background here is about 8×10^8 Janskys/steradian.

independent of the mass of the cloud. There appear to be no cases of uninhibited star formation. The star formation process appears to be equally efficient (or inefficient) in clouds of mass as low as 5×10^4 or as high as 5×10^6 $M_\odot$. This is evidence against nonlinear processes within a cloud, such as star-formation-induced star formation or supernova-induced star formation. Both of these processes would lead to a higher rate of star formation in the most massive clouds since the probability of forming a star per unit of available mass would be proportional to the number of recently-formed stars in the cloud. In fact, Figure 7 shows that there are many massive giant molecular clouds with no more than one O star. Twelve of the clouds in Figures 6, 7, and 8 (indicated by open circles) have no obvious IR sources; for these clouds the infrared luminosity should be regarded as an upper limit and there are probably no O stars. There are thus some giant molecular clouds with very little or no massive star formation.

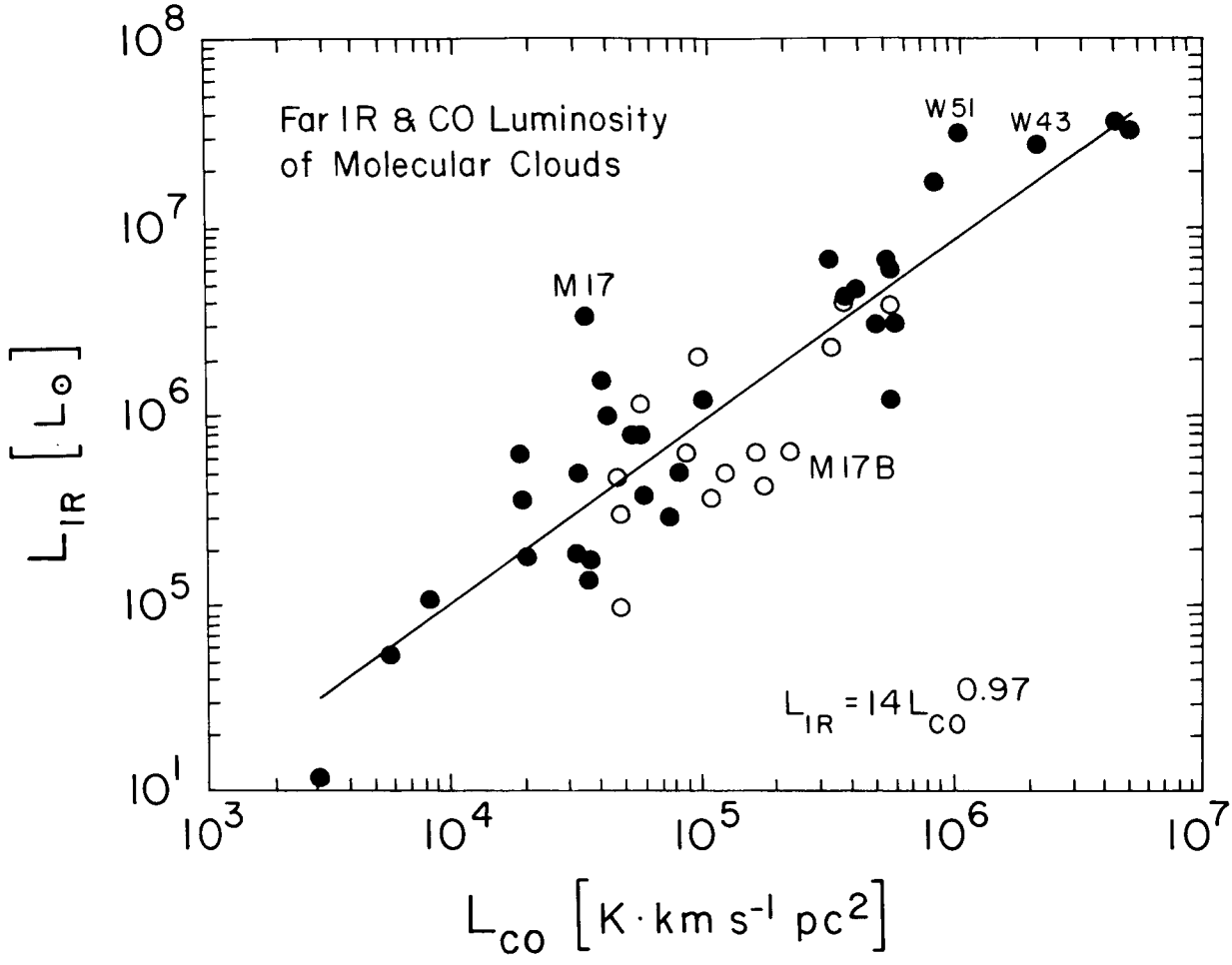

Figure 6. Far infrared luminosity as a function of CO luminosity for 46 molecular clouds in the galactic plane. The solid circles are molecular clouds with well defined IR sources which are H II regions associated with the cloud. The open circles are molecular clouds with no obvious IR.

Figure 8 shows the luminosity-to-mass ratio as a function of the far infrared color, F_{100}/F_{60}. The systematic decrease in the luminosity-to-mass ratio with decreasing far infrared color temperature is expected for thermal radiation. Expressed in terms of dust color temperature T_d we find, assuming an infrared emissivity proportional to the 1.5 power,

$$\left(\frac{L_{IR}}{M_{cloud}}\right) \propto (T_d)^{5.5}.$$

Thus the primary effect resulting in strong far infrared luminosity is simply hotter dust rather than more dust. Not surprisingly the far infrared emission at these wavelengths is not a good tracer of the mass of interstellar dust since there are some very massive cold clouds (see Figures 7 and 8) with relatively little far IR, such as M17B.

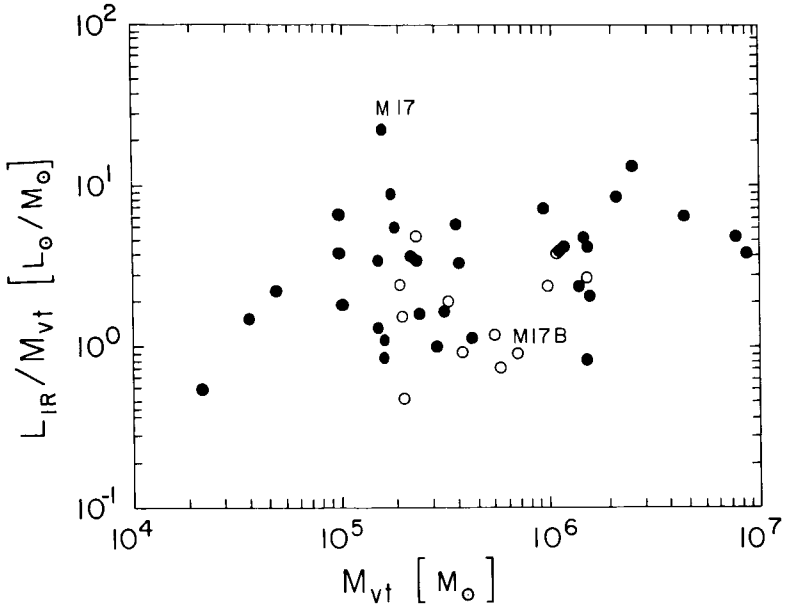

Figure 7. The ratio of infrared luminosity to cloud mass as a function of cloud mass. The solid and open circles are same as Figure 6. The star formation rate per unit of available molecular mass as measured by L_{IR}/M_{VT} is independent of the mass of the cloud.

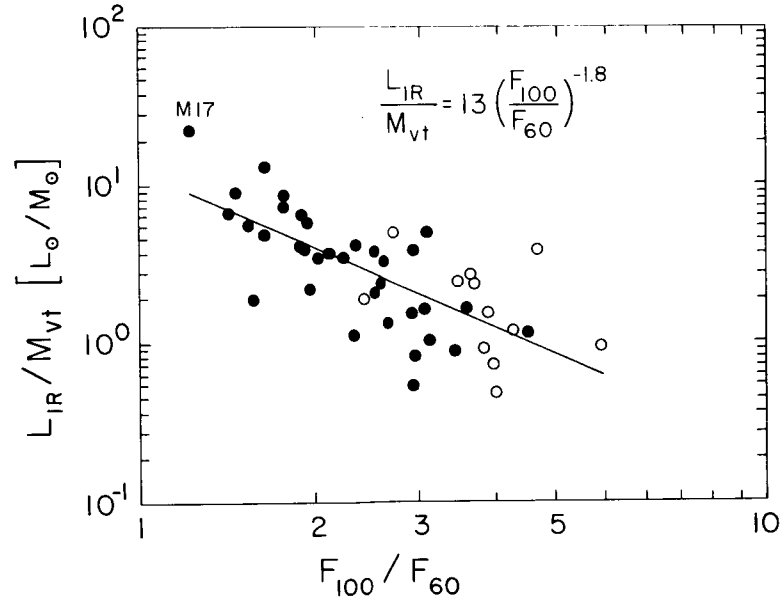

Figure 8 The ratio of infrared luminosity to cloud mass as a function of infrared color. The solid and open circles are the same as Figures 6 and 7. An emissivity $\varepsilon \propto \lambda^{-1.5}$ is assumed.

5. Galactic Plane IR–CO Emission

Figure 9 shows the 100 micron and CO flux from a region 1° in ℓ by 2° in b as a

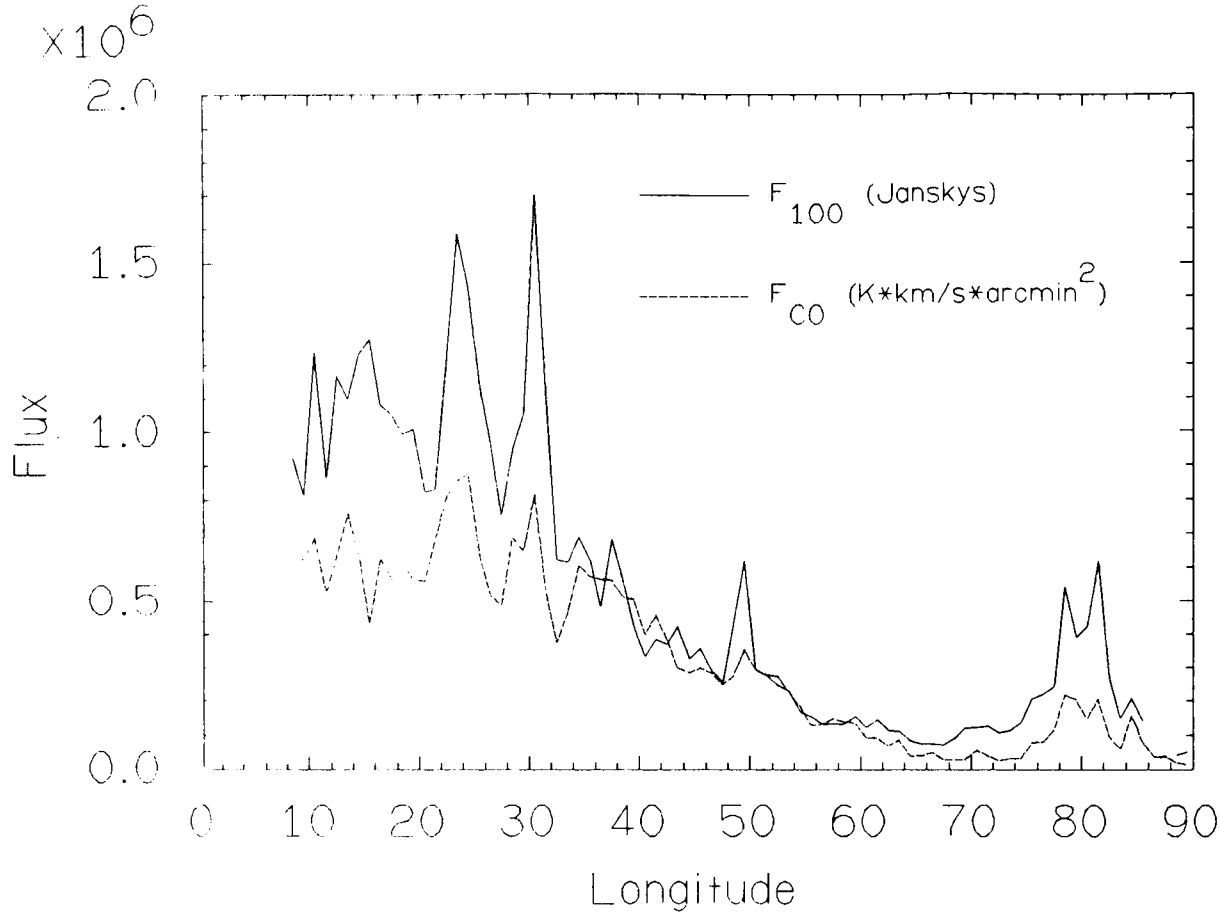

Figure 9. The 100 μm and CO flux binned every 1° in ℓ between $b = -1^\circ$ to $+1^\circ$, as a function of galactic longitude. The strong peaks near 23°, 31°, 50°, and 80° correspond to prominant molecular clouds in the galaxy (see text). The general trend with ℓ of the 100 μm and CO flux indicate that the molecular ring is a major feature of the *IRAS* data.

function of galactic longitude between the latitude range of $+1^\circ$ and -1°. The peaks in longitude and the general trend in longitude are the same for the 100 micron and CO flux. The strong peaks correspond to the most luminous molecular clouds in the galaxy located at (ℓ, b, v) : $(23.0, -0.4, 74)$ at a distance of $D = 12$ kpc, W43 $(30.8, -0.05, 92)$ at $D = 7$ kpc, and W51 $(49.5, -0.4, 57)$ at $D = 7$ kpc. Their IR luminosities are all about 4×10^7 $L_\odot$. The peak at $\ell \sim 80^\circ$ is from the relatively nearby Cygnus clouds. The fall off beyond longitudes of 35° is a characteristic not shared by the 21 cm emission from atomic hydrogen. Thus the molecular ring is clearly a major feature of the *IRAS* data as well as the CO data. On the basis of our assignments of infrared luminosity to molecular clouds, we estimate that about half of the far infrared flux is associated with the molecular component.

6. Face-on Picture of Warm Molecular Clouds in the Milky Way

Figure 10a is a face-on picture between $\ell = 8°$ and 90°, of the distribution of molecular clouds that we have found from the Massachusetts–Stony Brook CO Galactic Plane Survey and the Cloud Catalog discussed previously. Small and low luminosity clouds have been left out of this picture. The most prominent feature is the ring-like structure at about $R = 5$ kpc (we assume $R_0 = 10$ kpc) which is seen here to wind around to the far side of the galaxy at a distance of 14 kpc from the sun. Almost one-half of the CO luminosity in the warm component is in this feature, which corresponds to the traditional Scutum spiral arm tangent to the line of sight at a longitude near 30°. There are two other ring-like structures at approximately 7 kpc and 9 kpc from the galactic center which appear merged together on the far side of the galaxy. The 7 kpc feature is the well known Sagitarius spiral arm which is seen here to continue on to the far side of the galactic plane. While the accuracy of kinematic distances does not allow a conclusive statement regarding the pitch angle of these arms, their reality will remain regardless of distance errors due to noncircular motions such as streaming. In particular, the gap between $R = 6$ and 7 kpc is very prominent and appears even in the radial distribution of these objects (see Solomon, Sanders and Rivolo, 1985). Figure 10b is similar to Figure 10a but with the size of the molecular cloud image in proportion to the size of the molecular cloud. This gives a much more realistic appreciation of the space between the GMC's. Although the GMC's are the largest and most massive objects in the galaxy, the space between them or between the clusters of GMC's is much larger than their size.

It is important to note that these clouds represented in the picture are primarily those with peak intensities $T_R^* > 5$ K. As we have previously shown from an analysis of CO sources, these are the spiral arm population. The cold clouds which are more difficult to define by their outer boundaries, would fill in the spaces between the spiral arms just as the cold CO sources fill in the longitude velocity space (see Solomon, Sanders and Rivolo, 1985). Approximately one half of the galactic CO emission is in the warm clouds.

7. The Ratio of Far IR Luminosities to Molecular Mass in Interacting and Isolated Galaxies

As part of a program to investigate the content and distribution of molecular gas in external galaxies, we have observed λ 2.6 mm CO emission along the major axis of approximately 100 galaxies. In this section we briefly describe the results of a comparison of the CO and far infrared luminosities of these galaxies. We compare the results found for these external galaxies with those of molecular clouds in our own galaxy discussed in previous sections. The candidate galaxies were drawn from three separate samples. The first was a study of nearby large angular size spiral galaxies generally of type Sb or later with optical diameters greater than 7 arc minutes and distances greater than 4 Mpc. The second sample was drawn from early *IRAS* Circulars, particularly Circular 15. The third

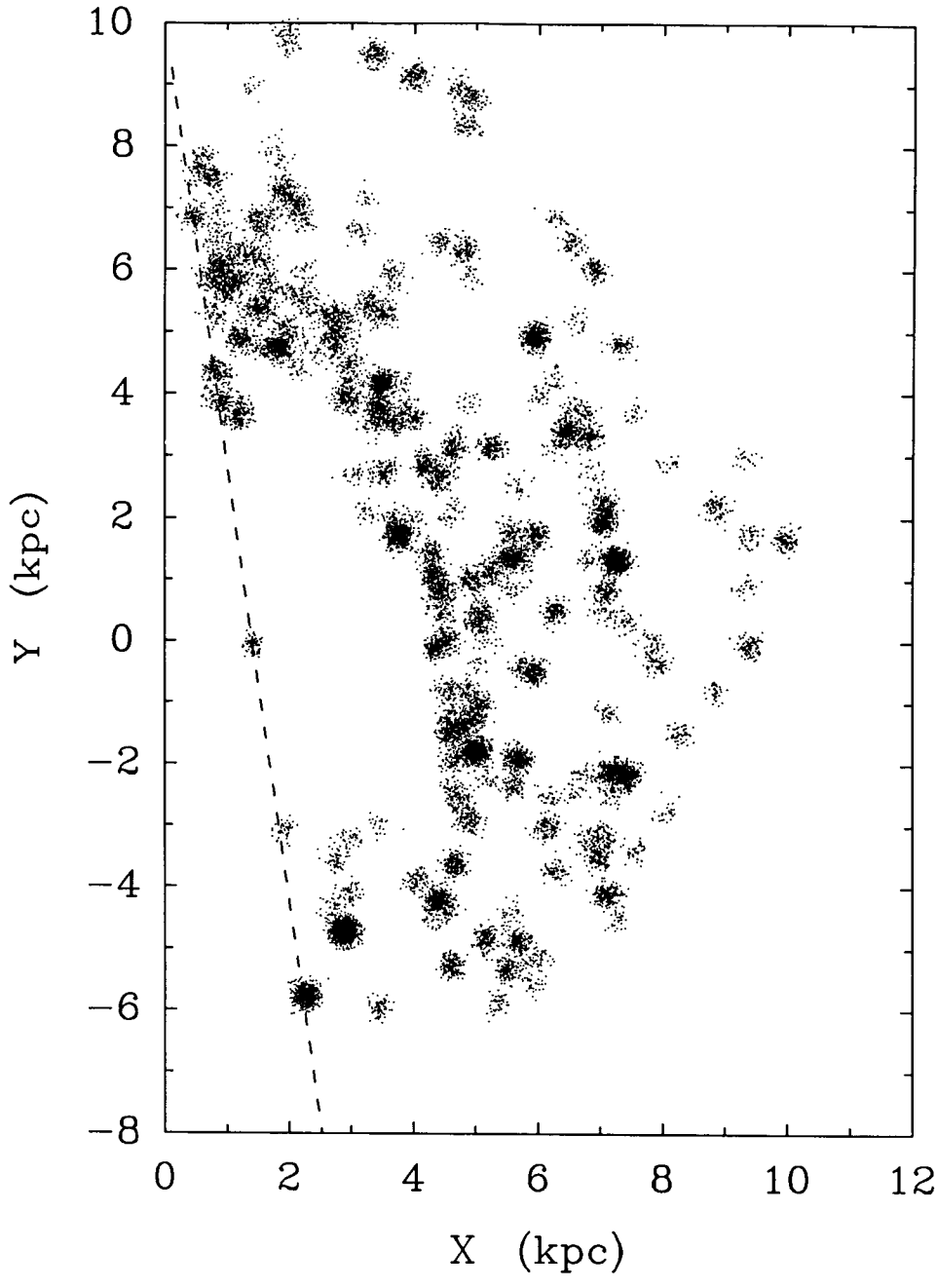

Figure 10a. Unresolved face-on picture of molecular clouds in the galaxy between $\ell = 8^\circ$ to 90°. The grey scale was generated with a Gaussian distribution of N points with $\sigma = 100$ pc about each cloud peak location. The contrast is achieved by setting $N = 150\,(L/10^5)^{0.75}$. The dashed line is the low longitude cutoff. Clouds with $L_{CO} < 1{\times}10^4$ $L_\odot$ were excluded.

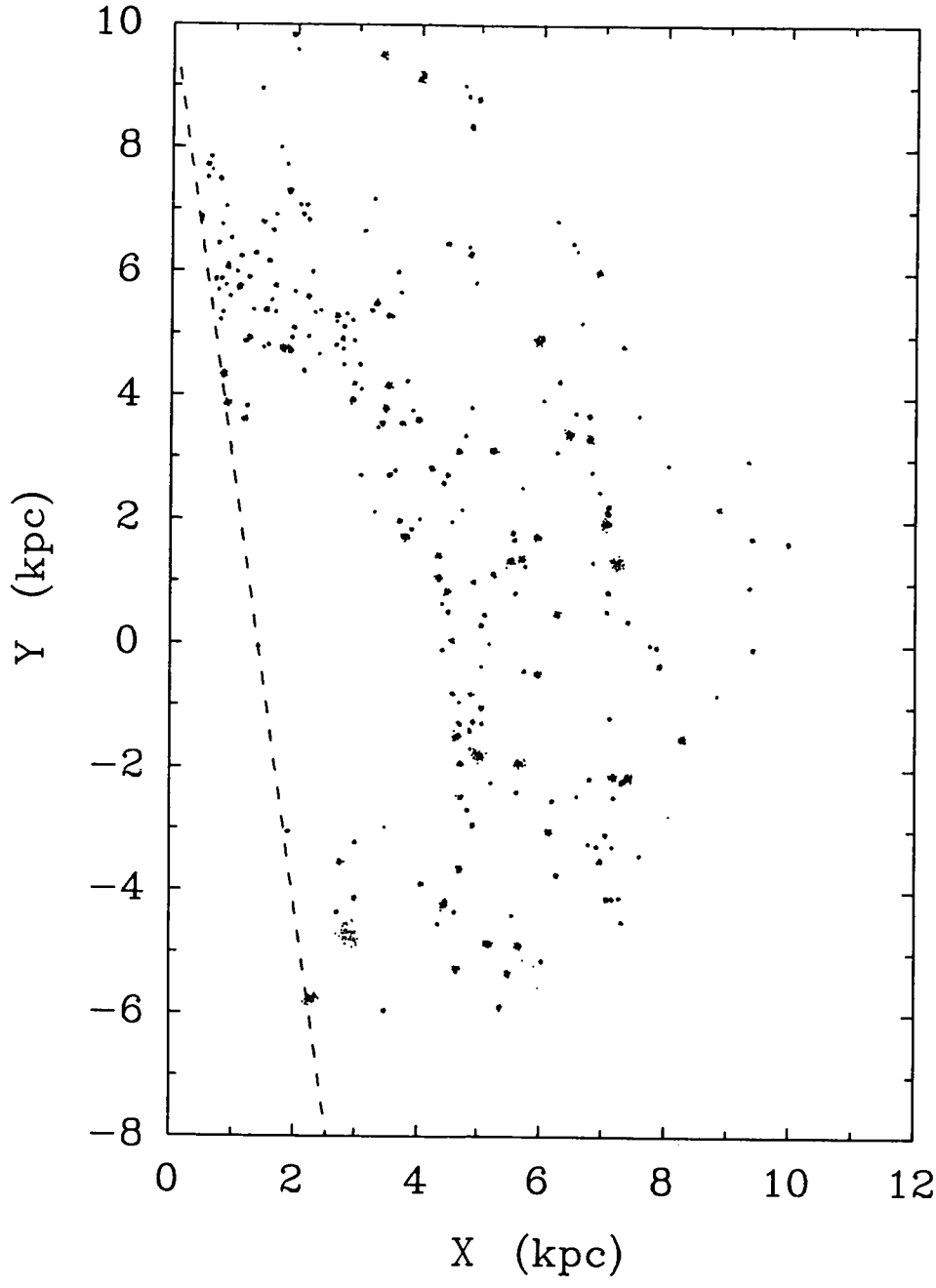

Figure 10b. Resolved face-on picture of the galaxy with same clouds as in figure 10a. The grey scale was fixed at 20 points per cloud with the size dispersion σ equal to the size dispersion of the clouds S.

sample consists of all *IRAS* galaxies at declination $\delta > 0°$, 100 μm flux > 30 Janskys and velocity $v > 700$ km $\cdot$ s^{-1}. The observations were carried out using primarily the FCRAO 14 meter antenna between 1982 and 1986 and more recently the NRAO 12 meter antenna. These observations are reported in detail elsewhere (Solomon, Sage and Barrett, 1986 and Sage, 1987). Previous studies but with smaller samples have been carried out by Sanders and Mirabel (1985) and Young *et al.* (1986).

Galaxies were classified as either isolated, interacting or merging based on their optical appearance. Interacting galaxies are those with disturbed appearances and/or neighbors closer than about 7 optical diameters. Merging galaxies are those with 2 nuclei as well as some of the extremely luminous peculiar galaxies such as MKN231, ARP220 and N6240. The combined sample has almost a 3 order of magnitude range in infrared flux.

Figure 11 shows the far infrared luminosity as a function of the CO luminosity for approximately 80 of these galaxies, both interacting and isolated. The CO luminosity was calculated from the major axis observations spaced every beamwidth taking account of the inclination of the galaxy and integrating out to at least half of the Holmberg radius. The far infrared luminosity was determined from the 60 and 100 μm fluxes in either the *IRAS* point source or extended source catalog. For large angular size nearby galaxies the far infrared luminosity was determined from the *IRAS* images.

As can be seen from Figure 11, there is generally a good correlation of the IR and CO luminosities but with a wide dispersion. The interacting galaxies are systematically higher in their infrared to CO ratio than the isolated galaxies although there is significant overlap between the two groups. In Figure 11 two lines have been drawn which indicate the range of the IR to CO ratio for galactic clouds. While many of the isolated galaxies could be understood as a collection of molecular cloud–H II regions similar to those in the galaxy, it is clear that the interacting, and particularly the merging galaxies, have IR to CO ratios substantially greater than any individual clouds in the Milky Way. Even some of the isolated galaxies appear a factor of two higher in this ratio than any clouds in our galaxy. This however could be explained if our galaxy has only about half of its far infrared emission associated with GMC's.

Figure 12 shows the infrared and CO luminosities separately for interacting and isolated galaxies along with a fit to the data. The interacting galaxies are systematically higher in the IR to CO ratio than the isolated galaxies by a factor of 3–5 with extreme cases such as MKN231 and ARP220 higher than the isolated galaxies by a factor of 10 to 20. If we utilize a constant conversion factor to obtain the molecular mass from the CO luminosity and regard the far infrared luminosity as an indicator of recent star formation, then we find that the star formation rate per unit mass of molecular hydrogen (as indicated by $L_{IR}/M(\mathrm{H_2})$) is 3–5 times greater in interacting than isolated galaxies.

The interacting, and particularly the merging, galaxies are also systematically hotter than the isolated galaxies. The merging galaxies in our sample have an average dust temperature (assuming a λ^{-1} emissivity) of $\sim$ 45 K while the isolated galaxies have an

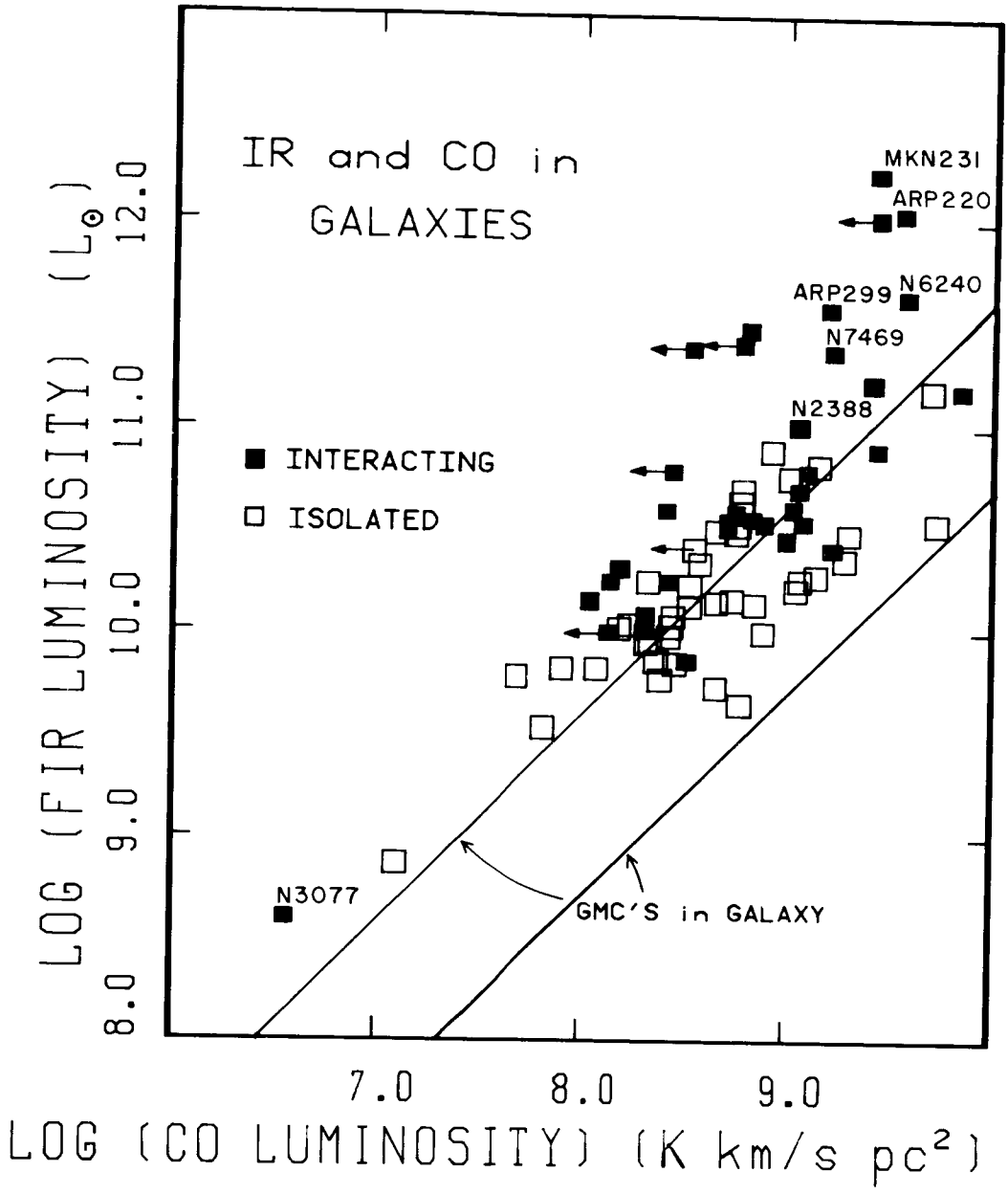

Figure 11. The Infrared and CO Luminosity of isolated and interacting galaxies. The two lines represent the range of L_{IR}/L_{CO} for the galactic molecular clouds. The interacting galaxies are systematically above the galactic GMC's.

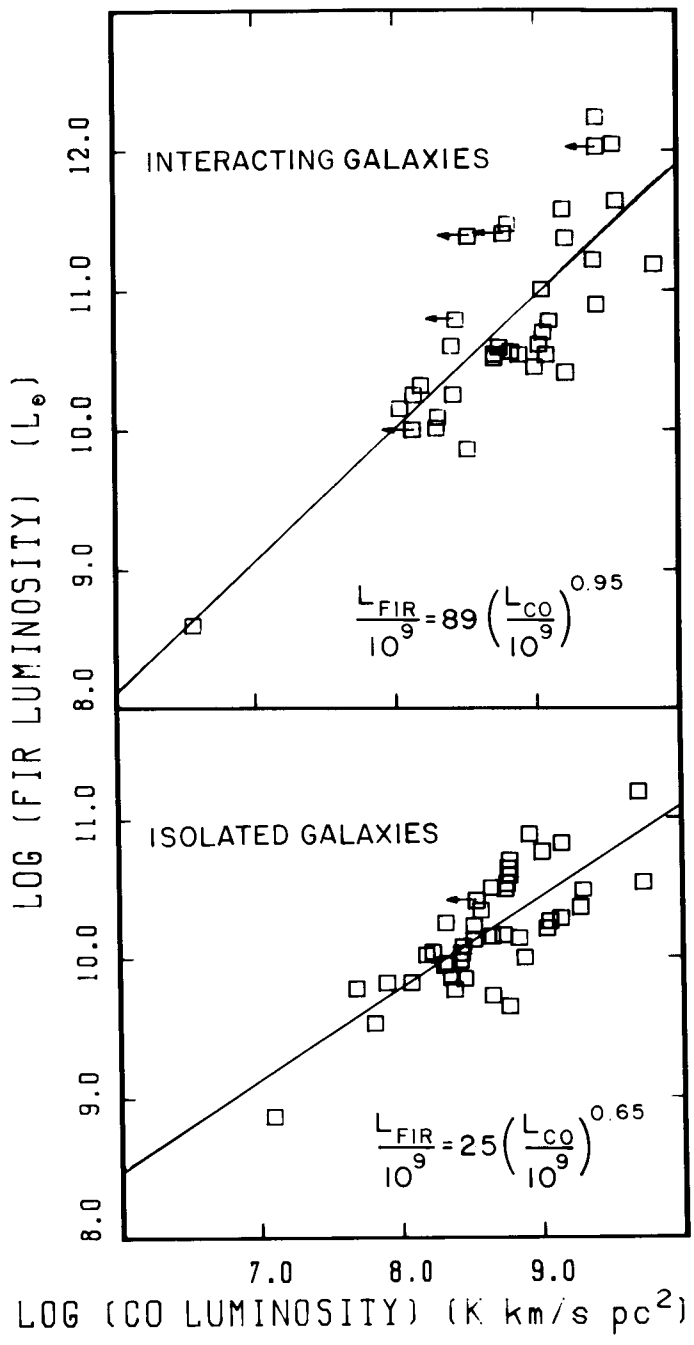

Figures 12a,b The Infrared and CO Luminosities separately with fits for a) interacting galaxies and b) isolated galaxies. The interacting galaxies are 3 to 5 times more luminous per unit of molecular mass (see text). The difference in the exponents of the fits needs to be tested with larger samples.

average dust temperature of $\sim$ 33 K. Much of the dispersion in $L_{IR}/M(H_2)$ is thus due to dust temperature variations since $L_{IR} \propto (T_d)^5$. Young *et al.* (1986) have treated the dust temperature as an independent parameter and fit the $L_{IR}/M(H_2)$ relation separately for galaxies of different temperature. However, the temperature dependence of L_{IR} on dust temperature is a necessary consequence of thermal radiation and selecting on dust temperature is almost equivalent to selecting on luminosity.

The dust temperature is therefore a result of the high luminosity and not a cause. We note that if the gas in the molecular clouds is also systematically hotter in interacting galaxies the CO–H_2 conversion factor will be smaller and $L_{IR}/M(H_2)$ will be even higher.

We thus find that the effect of an interaction appears to be to increase the star formation rate within preexisting molecular clouds rather than primarily creating new molecular clouds. Our finding that none of the molecular clouds in our galaxy has as high a ratio of IR to CO as the interacting or merging galaxies suggests a fundamental change in the star formation initiating mechanism in galaxy interactions.

8. Summary

From an analysis of several hundred galactic molecular clouds we have shown:

1) the velocity linewidth is propotional to the 0.5 power of the size $\sigma_v \propto (S)^{0.5}$. Combined with virial equilibrium this shows the clouds are characterized by a constant mean surface density and have a mass $M \propto {\sigma_v}^4$.

2) The virial mass–CO luminosity law is $M \propto (L_{CO})^{0.81}$. This establishes a calibration for measuring the total cloud mass from CO observations.

3) Molecular clouds are in or near virial equilibrium since their mass per unit CO luminosity determined dynamically, agrees with other measurements. The cloud CO luminosity $L_{CO} \propto {\sigma_v}^5$. This is the molecular cloud version of the Fisher-Tully or Faber-Jackson law for galaxies.

4) The far IR luminosity per unit cloud mass L_{IR}/M is independent of the cloud mass. Since the source of the far IR luminosity is primarily young massive stars, this argues against star formation induced star formation which is a nonlinear process that should spread throughout a cloud. There are some giant molecular clouds of mass 10^5–10^6 $M_\odot$ with little or no embedded far IR sources (O or early B stars).

5) Star formation activity is well regulated in galactic molecular clouds with a maximum (IR luminosity / cloud mass) ratio observed.

From an analysis of CO and far IR obsevations of external galaxies we conclude:

6) The fir IR luminosity and CO luminosity are well correlated but with a wide dispersion.

7) Interacting galaxies have systematically higher IR luminosities per unit molecular mass than isolated galaxies and more importantly have higher $L_{IR}/M(H_2)$ ratios than any galactic molecular clouds. This indicates that the star formation mechanism in interacting

and particularly merging galaxies is substantially more efficient than even the most active molecular cloud–H II region complexes in the galaxy. Star formation still appears as a viable mechanism for the luminous IR galaxies since the efficiency need only be enhanced by about one order of magnitude. The increase in efficiency may possibly be due to a compression of existing molecular clouds by cloud-cloud collisions during the interaction. The lack of efficient or even runaway star formation in giant molecular clouds in the galactic disk may be just as hard to explain as a "starburst" in luminous IR galaxies. Both systems have more than sufficient material in molecular clouds to account for their observed star formation.

References

Bhat, C. L., Issa, M. R., Houston, B. P., Mayer, C. J., and Wolfendale, A. W. 1985 *Nature* **314**, 511.

Blitz, L., and Shu, F. H. 1980 *Ap. J.* **238**, 148.

Bloemen, J. B. G. M., Caraveo, P. A., Hermsen, W., Lebrun, F., Maddalena, R. J., Strong, A. W., and Thaddeus, P. 1984 *Astron. Astrophys.* **139**, 37.

Bloemen, J. B. G. M., Strong, A. W., Blitz, L., Cohen, R. S., Dame, T. M., Grabelsky, D. A., Hermsen, W., Lebrun, F., Mayer-Hasselwander, H. A., and Thaddeus, P. 1986 *Astron. Astrophys.* **154**, 25.

Bronfman, L., Cohen, R. S., Alvarez, H., May, J., and Thaddeus, P. 1986 *preprint.*

Clemens, D. P., Sanders, D. B., Scoville, N. Z., and Solomon, P. M. 1986 *Ap. J. Suppl.* **60**, 297.

Dickman, R. L. 1975 *Ap. J.* **202**, 50.

Downes, D., Wilson, T. L., Bieging, J., and Wink, J. 1980 *Astron. Astrophys Suppl. Ser.* **40**, 379.

Gordon, M. A., and Burton, W. B. 1976 *Ap. J.* **208**, 346.

Liszt, H. S., and Burton, W. B. 1981 *Ap. J.* **243**, 778.

Liszt, H. S. 1982 *Ap. J.* **262**, 198.

Sage, L. J. 1987 *thesis, in preparation*

Sanders, D. B., Clemens, D. P., Scoville, N. Z., and Solomon, P. M. 1986 *Ap. J. Suppl.* **60**, 1.

Sanders, D. B., Mirabel, I. F. 1985 *Ap. J.* **298**, L31.

Sanders, D. B., Scoville, N. Z., and Solomon, P. M. 1985 *Ap. J.* **289**, 373.

Sanders, D. B., Solomon, P. M., and Scoville, N. Z. 1984 *Ap. J.* **276**, 182.

Scoville, N. Z., and Solomon, P. M. 1975 *Ap. J. (letters)* **199**, L105.

Solomon, P. M., Rivolo, A. R., Barrett, J. W., and Yahil, A. 1986a *submitted to Ap. J.*

Solomon, P. M., Sage, L. J., Barrett, J. W. 1986 *submitted to Ap. J.*

Solomon, P. M., Sanders, D. B., and Scoville, N. Z. 1979 In *IAU Symposium 84, The Large Scale Characteristics of the Galaxy*, ed. W. B. Burton (Dordrecht: Reidel), p. 35.

Solomon, P. M., and Sanders, D. B. 1980 In *Giant Molecular Clouds in the Galaxy*, eds. P. M. Solomon and M. G. Edmunds, (New York:Pergamon), pp. 41.

Solomon, P. M., Sanders, D. P., and Rivolo, A. 1985 *Ap. J.* (*letters*) **292**, L19.

Solomon, P. M., Sanders, D. B., Scoville, N. Z., and Clemens, D. P. 1986b *Ap. J. Suppl.* (*in press*).

Thaddeus, P., and Dame, T. M. 1984 Proceedings of Workshop on Star Formation, in *Occasional Reports of Royal Observatory, Edinburgh*, ed. R. Wolstencroft.

Young, J. S., Kenney, J., Lord, S. D. and Schloerb, F. P. 1984 *Ap. J.* **287**, L65.

Young, J. S., Schloerb, F. P., Kenney, J. D. and Lord, S. D. 1986 *Ap. J.* **304**, 443.